

## INFLUENCE OF THERMAL ANNEALING ON THE STRUCTURAL AND OPTICAL PROPERTIES OF POLYCRYSTALLINE $\text{Cd}_{0.96}\text{Zn}_{0.04}\text{Te}$ THIN FILMS

M. G. Sridharan<sup>\*</sup>, Sa. K. Narayandass, D. Mangalaraj, H. Chul Lee<sup>a</sup>

Thin Film Laboratory Department of Physics, Bharathiar University, Coimbatore – 641 046, India

<sup>a</sup>Department of Electrical Engineering and Computer Science, Korea Advanced Institute of Science and Technology, Taejon – 305 701, Korea

The influence of thermal annealing on the structural and optical properties of  $\text{Cd}_{0.96}\text{Zn}_{0.04}\text{Te}$  thin films were studied by XRD, AFM, optical transmittance measurement and Raman scattering. The polycrystalline  $\text{Cd}_{0.96}\text{Zn}_{0.04}\text{Te}$  films were deposited onto well-cleaned glass substrates (Corning 7059) maintained at room temperature and are annealed. The films were stoichiometric as analyzed by RBS and EDAX. The films exhibited zinc blende structure with predominant  $\langle 111 \rangle$  orientation. The intensity of the  $\langle 111 \rangle$  peak increases and the FWHM decreases on thermal annealing. The rms roughness of the as-deposited film is 3.7 nm and the value decreases on annealing. The direct allowed band gap value of the room temperature deposited films is 1.523 eV which decreases on thermal annealing. The Raman spectra of the films show longitudinal- and transverse-optical (LO, TO) modes, which arise from CdTe- and ZnTe-like vibrations. The intensity of the peaks increases and the FWHM decreases with the increase in annealing temperature indicates the improvement of crystallinity on thermal annealing.

(Received April 21, 2005; accepted May 26, 2005)

*Keywords:*  $\text{Cd}_{0.96}\text{Zn}_{0.04}\text{Te}$ , Structural properties, Optical properties, Raman scattering, Thin film

### 1. Introduction

$\text{Cd}_{1-x}\text{Zn}_x\text{Te}$  is a ternary IIB-VIA compound semiconductor, which is having promising applications in a variety of solid-state devices, such as solar cells, photo detectors and light emitting diodes, as the band gap is expected to be direct and tunable in the region between 1.45 and 2.3 eV (for  $x = 0$  and  $x = 1$  respectively) [1-4].  $\text{Cd}_{1-x}\text{Zn}_x\text{Te}$  is used in optical memory devices, X-ray and gamma ray detectors [5].  $\text{Cd}_{1-x}\text{Zn}_x\text{Te}$  material with a band gap of 1.65 – 1.75 eV is especially attractive for use in high efficient tandem solar cell structures [6]. Though much work has been published on the properties of bulk  $\text{Cd}_{1-x}\text{Zn}_x\text{Te}$  very limited information is available on  $\text{Cd}_{1-x}\text{Zn}_x\text{Te}$  thin films [7-10].  $\text{Cd}_{1-x}\text{Zn}_x\text{Te}$  ( $x = 0.04$ ) nearly lattice matches with  $\text{Hg}_{1-y}\text{Cd}_y\text{Te}$  (MCT) for all values of  $y$ , so it is mainly used as a substrate material for the epitaxial growth of MCT infrared focal plane arrays (IRFPAs) [11]. The main advantage of the  $\text{Cd}_{0.96}\text{Zn}_{0.04}\text{Te}$  is its infrared transparency, which allows backside illumination of the MCT infrared detector arrays [12]. Recently  $\text{Cd}_{1-x}\text{Zn}_x\text{Te}$  ( $x = 0.04$ ) is used as surface passivation layer for MCT infrared detectors [13, 14].

Thin films of  $\text{Cd}_{1-x}\text{Zn}_x\text{Te}$  were prepared by variety of techniques, such as, two source vacuum evaporation (TSVE), molecular beam epitaxy (MBE), chemical vapour deposition (CVD) and closed space vapour transport (CSVT) [15-17]. In the present study  $\text{Cd}_{0.96}\text{Zn}_{0.04}\text{Te}$  thin films are deposited by vacuum evaporation onto well-cleaned glass substrates (Corning 7059) maintained at room temperature and the films are characterized by several techniques like X-ray diffraction (XRD), Rutherford backscattering spectrometry (RBS), energy dispersive analysis of X-ray (EDAX), atomic force microscopy (AFM), optical transmittance and Raman scattering. Also the

<sup>\*</sup> Corresponding author: mgs\_sridharan@yahoo.com

films are annealed at 423 and 523 K and the effect of thermal annealing on the structural and optical properties of the  $\text{Cd}_{0.96}\text{Zn}_{0.04}\text{Te}$  films are discussed.

## 2. Experimental

### 2.1. $\text{Cd}_{0.96}\text{Zn}_{0.04}\text{Te}$ alloy preparation

The  $\text{Cd}_{0.96}\text{Zn}_{0.04}\text{Te}$  alloy was prepared from its own constitutional elements. Appropriate weights of Cd, Zn and Te (of purity 99.999%) were mixed together, charged in a quartz tube and sealed under a vacuum of  $10^{-5}$  Torr. The sealed quartz ampoule with the charge was placed in a rotating furnace. The temperature of the furnace was raised gradually to 1373 K and left at this temperature for about 36 hours, after that the ampoule was slowly cooled to room temperature at a rate of  $30^\circ\text{C/h}$  [18]. The  $\text{Cd}_{0.96}\text{Zn}_{0.04}\text{Te}$  ingot was taken out from the ampoule and made into fine powder.

### 2.2. Thin film deposition and characterization

Polycrystalline  $\text{Cd}_{0.96}\text{Zn}_{0.04}\text{Te}$  thin films were deposited onto well-cleaned glass substrates (Corning 7059) kept at room temperature by vacuum evaporation technique. Tantalum boat with the charge was used as the source and the pressure inside the chamber was maintained better than  $10^{-5}$  Torr. The thicknesses of the films were measured by multiple beam interference (MBI) technique [19]. Also the thicknesses of the films were verified with  $\alpha$ -Step (TENCOR  $\alpha$ -Step Instrument) measurement. The composition and the thicknesses of the films were evaluated by using Rutherford backscattering spectrometry (RBS). Energy dispersive X-ray analysis was used to confirm the film composition. The studies were carried out for a film of typical thickness 302 nm.  $\text{Cd}_{0.96}\text{Zn}_{0.04}\text{Te}$  films were annealed in vacuum for 1 hour at 423 and 523 K. Structural analysis was made using a Philips X-ray diffractometer with  $\text{CuK}\alpha$  radiation ( $\lambda = 1.542 \text{ \AA}$ ) at 40 kV and 20 mA in the scanning angle ( $2\theta$ ) from  $20^\circ$  to  $60^\circ$ . The surface microstructure of the films was investigated by ex-situ atomic force microscopy (AFM) (Park Scientific Instruments, Autoprobe CP Model). The AFM images were acquired in the tapping mode and in the repulsive force regime with a force constant of 1 nN between the AFM cantilever tip and the sample surface. The optical transmittance was recorded using an UV-VIS-NIR (SHIMADZU 3101 PC) spectrophotometer in the wavelength range 400-2000 nm. Raman spectroscopic technique is the most useful method available to study the lattice vibrations and their interactions with other excitations [20]. The Raman spectra of the  $\text{Cd}_{0.96}\text{Zn}_{0.04}\text{Te}$  films were recorded at room temperature using the 488 nm Argon ion laser beam of power 200 mW over a  $50 \mu\text{m}$  spot size. The scattered light was collected in the backscattering geometry using a double grating monochromator SPEX model 14018. A thermoelectrically cooled photomultiplier tube model ITT-FW 130 was used to detect the scattered light after passing through a monochromator [21]. The spectral resolution of the monochromator was about  $4.2 \text{ cm}^{-1}$ . The spectra were recorded using a microprocessor based automated data collection system with a step of  $0.5 \text{ cm}^{-1}$  and a collection time of 10 s.

## 3. Results and discussion

### 3.1. Thickness and composition

The vacuum evaporated  $\text{Cd}_{0.96}\text{Zn}_{0.04}\text{Te}$  films were found to be uniform and have very good adhesion to the substrate surface. The thickness of the films measured by MBI technique was  $300 \pm 1 \text{ nm}$ , which agrees well with the thickness measured from RBS technique ( $302 \pm 1 \text{ nm}$ ). The thicknesses of the films measured by  $\alpha$ -Step were  $303 \pm 1 \text{ nm}$ . Rutherford backscattering spectrum of vacuum evaporated  $\text{Cd}_{0.96}\text{Zn}_{0.04}\text{Te}$  films of thickness 302 nm is shown in Fig. 1. The film is found to have a very good stoichiometry as analyzed by the RBS simulation (GISA3) [Cd:46.04%, Zn:3.96%,

Te:50%]. The composition determined by EDAX do not vary much from RBS result and a typical EDAX spectrum of  $\text{Cd}_{0.96}\text{Zn}_{0.04}\text{Te}$  films is shown in Fig. 2. The ratio of II:VI elements was found to be 1:1. There was no significant change in the thickness and elemental composition of the films due to thermal annealing.

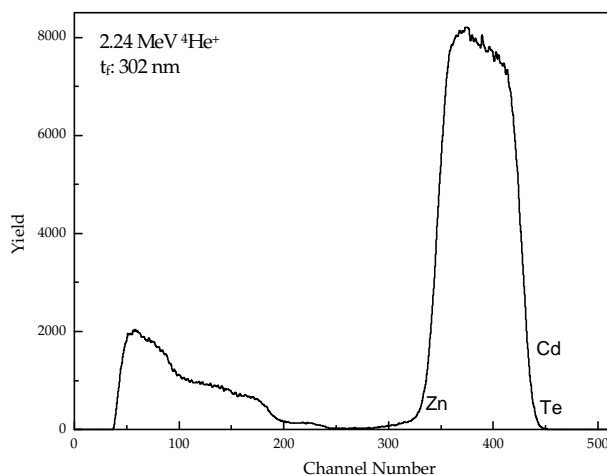


Fig. 1. Typical Rutherford backscattering spectrum of vacuum evaporated  $\text{Cd}_{0.96}\text{Zn}_{0.04}\text{Te}$  films.

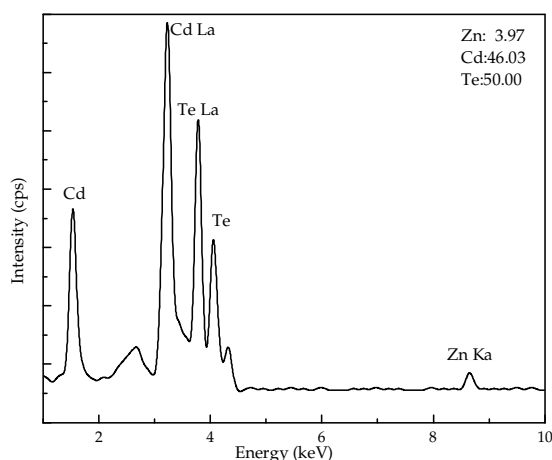


Fig. 2. EDAX spectrum of vacuum evaporated  $\text{Cd}_{0.96}\text{Zn}_{0.04}\text{Te}$  films.

### 3.2. X-ray diffraction analysis

The X-ray diffraction patterns of the as-deposited and annealed  $\text{Cd}_{0.96}\text{Zn}_{0.04}\text{Te}$  films are shown in Fig. 3.  $\text{Cd}_{0.96}\text{Zn}_{0.04}\text{Te}$  films were found to exhibit three diffraction peaks associated with  $\langle 111 \rangle$ ,  $\langle 220 \rangle$  and  $\langle 311 \rangle$  reflections, of which the intensity of the  $\langle 111 \rangle$  orientation is very predominant. The films exhibited zinc blende structure. The X-ray diffraction pattern of the films annealed at 423 and 523 K shows an increase in intensity of  $\langle 111 \rangle$  peak and a decrease in peak width (FWHM), which indicates an improvement in the crystallinity of the films on thermal annealing. Also on thermal annealing the intensity of the  $\langle 220 \rangle$  and  $\langle 311 \rangle$  peaks decreases.

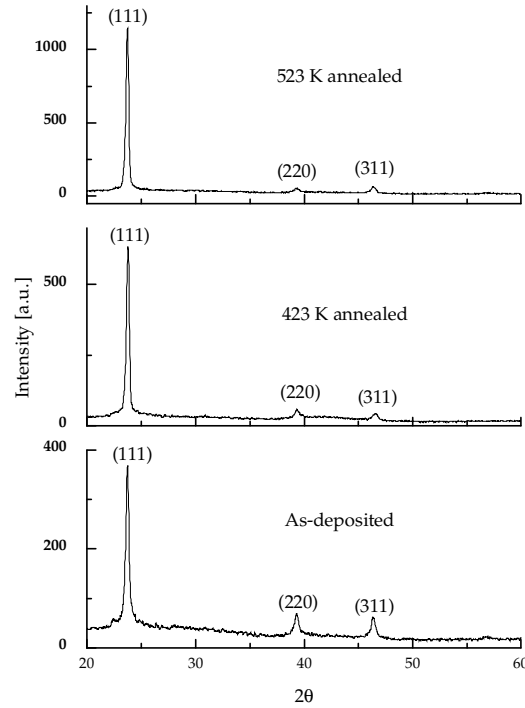


Fig. 3. X-ray diffraction patterns of vacuum evaporated  $\text{Cd}_{0.96}\text{Zn}_{0.04}\text{Te}$  thin films.

The lattice constant  $a$  of the vacuum evaporated  $\text{Cd}_{0.96}\text{Zn}_{0.04}\text{Te}$  films was determined by using the relation,

$$a = \frac{\lambda_x \sqrt{h^2 + k^2 + l^2}}{2 \sin \theta} \quad (1)$$

where,  $\lambda_x$  is the X-ray wavelength and  $\theta$  is the Bragg angle. The average grain sizes ( $D$ ) of the as-deposited and the annealed films were determined from the  $\langle 111 \rangle$  peak using the Scherrer formula,

$$D = \frac{0.94\lambda}{\beta \cos \theta} \quad (2)$$

where,  $\lambda$  is the X-ray wavelength,  $\beta$  is the full width at half maxima and  $\theta$  is the Bragg angle. The dislocation density of the films was determined using the relation,

$$\delta = \frac{1}{D^2} \quad (3)$$

The  $\text{Cd}_{0.96}\text{Zn}_{0.04}\text{Te}$  films exhibited zinc blende structure with lattice constant  $a = 6.459 \text{ \AA}$ . This value nearly matches with the lattice constant of  $\text{Hg}_{1-y}\text{Cd}_y\text{Te}$  ( $y = 0.22$ ) [11]. The grain size of the as-deposited film is about  $0.152 \text{ \mu m}$  whereas for the films annealed at 423 and 523 K the grain sizes are found to be  $0.157$  and  $0.164 \text{ \mu m}$  respectively. The dislocation density of the as-deposited films is  $4.33 \times 10^9 \text{ cm}^{-2}$  and for the films annealed at 423 and 523 K the dislocation densities were  $4.06 \times 10^9 \text{ cm}^{-2}$  and  $3.72 \times 10^9 \text{ cm}^{-2}$  respectively. The values are comparable with earlier reports [16, 22, 23].

### 3.3. Atomic force microscopy

Ex-situ atomic force microscope (AFM) has been used independently to access surface quality of the vacuum evaporated  $\text{Cd}_{0.96}\text{Zn}_{0.04}\text{Te}$  thin films. Fig. 4 shows the large scale ( $1\ \mu\text{m} \times 1\ \mu\text{m}$ ) two-dimensional and three-dimensional AFM images of the as-deposited and annealed films. The evaluated root mean square (rms) roughness of the as-deposited film was 3.7 nm and for the films annealed at 423 and 523 K was found to be 3.4 and 3.1 nm respectively (error  $\pm 0.1\ \text{nm}$ ), which indicates that the surface quality of the films increases on thermal annealing, which may be due to the removal of surface defects on thermal treatment.

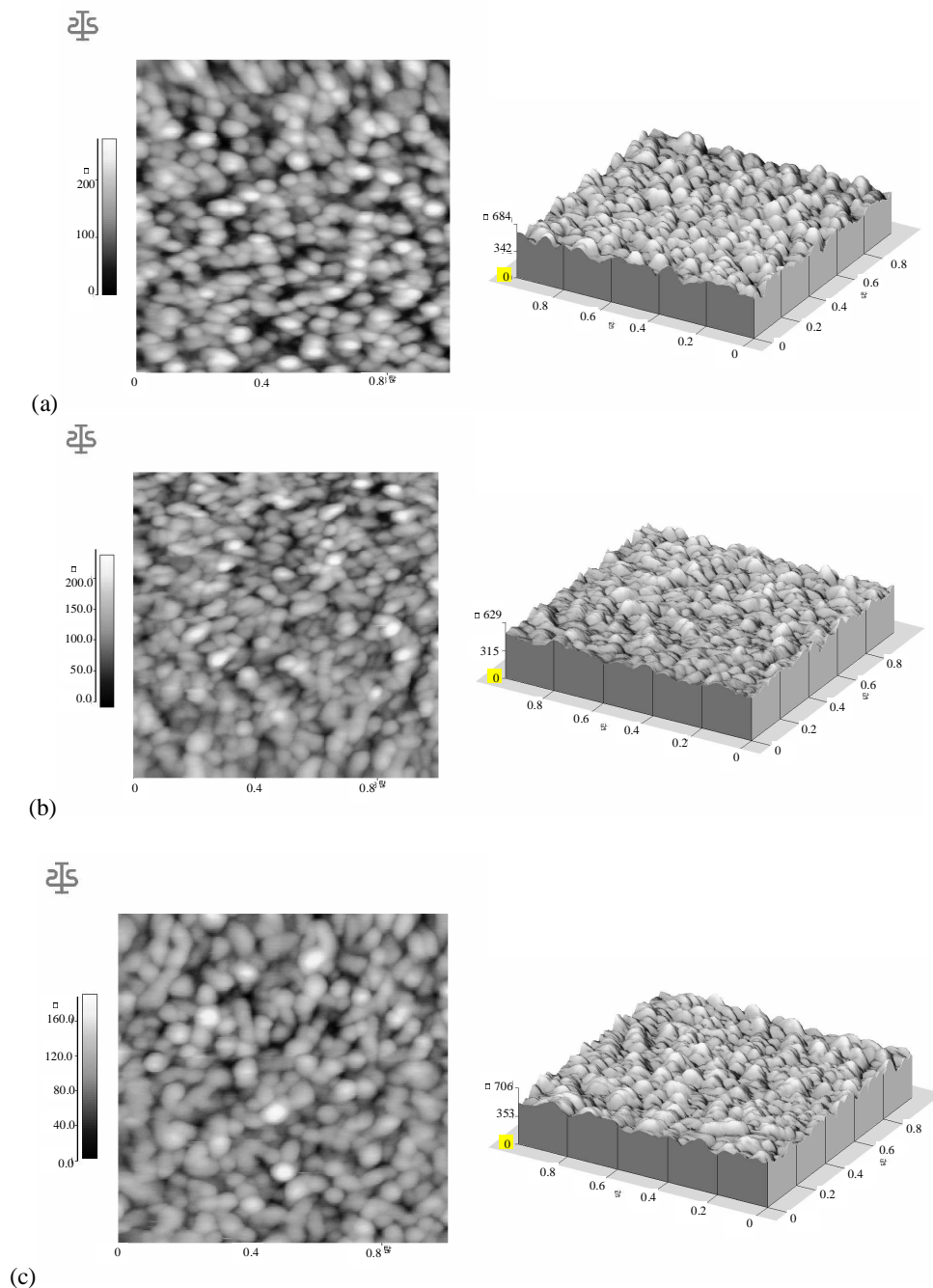


Fig. 4. Two dimensional and three-dimensional AFM images of vacuum evaporated  $\text{Cd}_{0.96}\text{Zn}_{0.04}\text{Te}$  thin films. (a) As-deposited (b) 423 K annealed (c) 523 K annealed.

### 3.4. Optical transmittance measurement

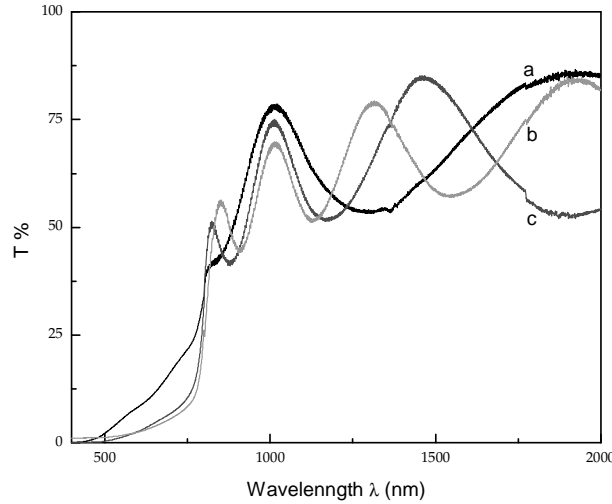


Fig. 5.  $\lambda$  vs T plot for vacuum evaporated  $\text{Cd}_{0.96}\text{Zn}_{0.04}\text{Te}$  films.

Fig. 5 shows the optical transmittance spectra of the as-deposited and annealed  $\text{Cd}_{0.96}\text{Zn}_{0.04}\text{Te}$  films in the wavelength range 400 – 2000 nm. The transmittance of the films is high at higher wavelength region. The transmittance spectra of the as-deposited and annealed films show interference patterns with a sharp fall of transmittance at the band edge, which indicates the crystallinity of the films. The variation of transmittance with wavelength is given by the relation [24]

$$T = \frac{16n_a n_g n^2 \exp(-\alpha t)}{R_1^2 + R_2^2 \exp(-\alpha t) + 2R_1 R_2 \exp(-\alpha t) \cos(4\pi n t / \lambda)} \quad (4)$$

where,  $\alpha$  is the absorption coefficient and  $n$ ,  $n_a$  and  $n_g$  are the refractive indices of the film, air and substrate respectively. The maxima and minima in the transmittance versus wavelength (T- $\lambda$ ) plot occur when,

$$\frac{4\pi n t}{\lambda} = M\pi \quad (5)$$

where,  $M$  represents the order number and  $t$  the thickness of the film. The refractive index  $n$  of the films has been computed using the relation [25, 26] given below,

$$n^2 = \frac{n_a^2 + n_g^2}{2} + 2n_a n_g T'' + \left[ \frac{(n_a^2 + n_g^2 + 4n_a n_g T'')^2}{4} - n_a^2 n_g^2 \right]^{1/2} \quad (6)$$

where,  $T'' = (T_{\max} - T_{\min}) / (T_{\max} + T_{\min})$ .  $T_{\max}$  and  $T_{\min}$  represent the envelopes of the maximum and minimum positions of the T- $\lambda$  curve.

The extinction coefficient  $k$  and the absorption coefficient  $\alpha$  of the films were calculated from the relations,

$$k = \frac{\ln(1/T)\lambda}{4\pi} \quad (7)$$

and

$$\alpha = \frac{4\pi k}{\lambda} = \frac{\ln(1/T)}{t} \quad (8)$$

where,  $t$  is the film thickness. The calculated values of  $n$  and  $k$  for the as-deposited films were plotted as a function of photon energy and are shown in Fig. 6. The value of refractive index  $n$  is found to decrease with increase of photon energy.

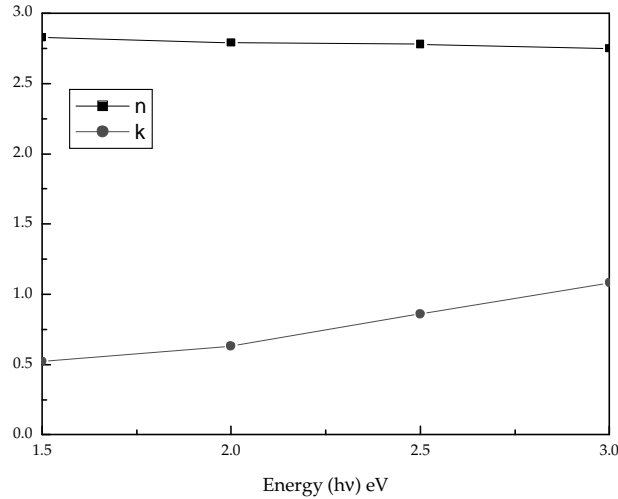


Fig. 6. Variation of  $n$  and  $k$  with photon energy for as-deposited  $\text{Cd}_{0.96}\text{Zn}_{0.04}\text{Te}$  films.

The absorption coefficient ( $\alpha$ ) is related to the band gap energy ( $E_g$ ) by using the relation [27],

$$\alpha = (h\nu - E_g)^{1/2} / h\nu \quad (9)$$

Fig. 7 shows the plot of  $(\alpha h\nu)^2$  versus  $h\nu$  of the as-deposited and 423 and 523 K annealed films. The optical band gap values were obtained by extrapolating the linear portion of the plot of  $(\alpha h\nu)^2$  versus  $h\nu$  to  $\alpha=0$ . The band gap value of the as-deposited film is found to be 1.523 eV. The value is in good agreement with the earlier report [16]. The band gap values are found to be decreasing with increase in annealing temperature. The band gap for 423 and 523 K annealed films are 1.503 and 1.481 eV respectively. The decrease of band gap may be due to increase in the grain size of  $\text{Cd}_{0.96}\text{Zn}_{0.04}\text{Te}$  during thermal annealing [28]. The structural parameters and the optical band gap of the as-deposited and 423 and 523 K annealed films are given in Table 1.

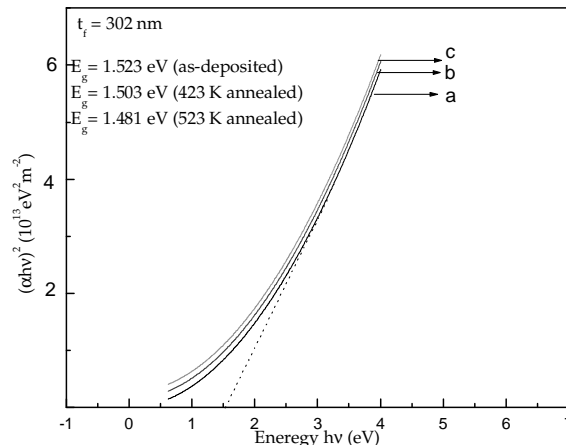


Fig. 7. Plot of  $(\alpha h\nu)^2$  vs  $h\nu$  for the  $\text{Cd}_{0.96}\text{Zn}_{0.04}\text{Te}$  thin films.

Tabl. 1. Structural parameters and optical band gap values of vacuum evaporated  $\text{Cd}_{0.96}\text{Zn}_{0.04}\text{Te}$  films ( $t_f$ : 302 nm).

Film	rms roughness (nm)	Grain size(D) ( $\mu\text{m}$ )	Dislocation density ( $\delta$ ) $\times 10^9 \text{ cm}^{-2}$	Band gap ( $E_g$ ) (eV)
As-deposited	3.7	0.152	4.33	1.523
423 K annealed	3.4	0.157	4.06	1.503
523 K annealed	3.1	0.164	3.72	1.481

### 3.5. Raman scattering spectrometry

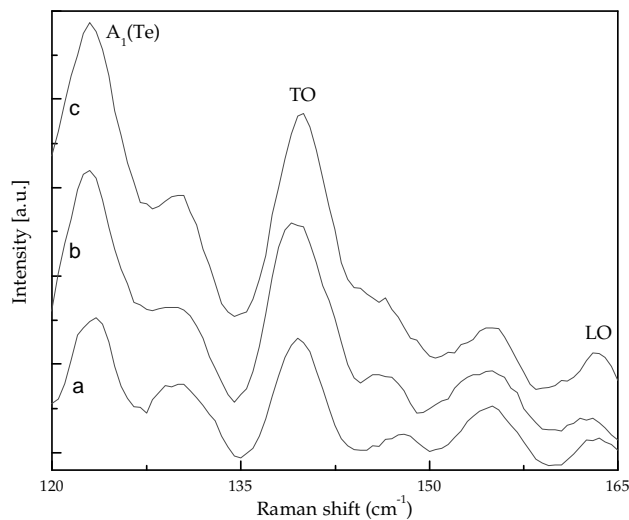


Fig. 8. Raman spectra of Vacuum evaporated  $\text{Cd}_{0.96}\text{Zn}_{0.04}\text{Te}$  thin films.

Fig. 8 shows the typical Raman spectra of the as-deposited and annealed  $\text{Cd}_{0.96}\text{Zn}_{0.04}\text{Te}$  thin films. The Raman spectra of the films show longitudinal- and transverse-optical (LO, TO) modes, which arise from CdTe- and ZnTe-like vibrations. The Raman peaks are identified at  $139.88 \text{ cm}^{-1}$  and  $163.40 \text{ cm}^{-1}$  for the transverse optic (TO) and the longitudinal optic (LO) phonons respectively in  $\text{Cd}_{1-x}\text{Zn}_x\text{Te}$  [29]. The peak at  $123 \text{ cm}^{-1}$  is the phonon with  $A_1$  symmetry of the Te precipitates in CdTe [30]. The origin of the peak at  $157 \text{ cm}^{-1}$  is not fully understood but could be the phonon with symmetry E seen in the Te single crystals at  $147 \text{ cm}^{-1}$  [30]. In the case of annealed films, the change in the Raman peak position is not much significant, but the intensity of the peaks increases with the increase in annealing temperature and the FWHM is found to be decreased. The increase in the peak intensity and the decrease of FWHM was due to the improvement in the crystallinity of  $\text{Cd}_{0.96}\text{Zn}_{0.04}\text{Te}$  films on thermal annealing.

### 4. Conclusions

$\text{Cd}_{0.96}\text{Zn}_{0.04}\text{Te}$  thin films were deposited by vacuum evaporation technique onto well-cleaned glass substrates. The films exhibited good stoichiometry as analyzed by RBS and EDAX. The films exhibited zinc blende structure with predominant  $\langle 111 \rangle$  orientation. The lattice constant of the

Cd<sub>0.96</sub>Zn<sub>0.04</sub>Te thin films is 6.459 Å, which nearly matches the lattice constant of Hg<sub>1-y</sub>Cd<sub>y</sub>Te (y = 0.22). The rms roughness of the as-deposited Cd<sub>0.96</sub>Zn<sub>0.04</sub>Te thin films was 3.7 nm and on annealing the films at 523 K the rms roughness value decreases to 3.1 nm, which may be due to the removal of surface defects on thermal treatment. The band gap of the as-deposited film was 1.523 eV and for the thermally annealed films the band gap value is found to be decreased. This decrease of band gap energy can be attributed to the increase of grain size during thermal annealing. The Raman spectra of the as-deposited films confirm the crystallinity of the films. The increase in the peak intensity and the decrease in FWHM of the Raman peak for the annealed films indicate the improvement in the crystallinity of the films during thermal annealing.

### References

- [1] T. Chikamura, S. Fujiwara, M. Fukai, *J. Appl. Phys.* **52**, 5146 (1982).
- [2] P. J. Dean, *J. Lumin.* **18-19**, 755 (1979).
- [3] N. G. Patel, *J. Mater. Sci.* **21**, 2097 (1986).
- [4] G. A. Thomas, V. B. Timofeev in *Optical properties of solids, Hand book on Semiconductors, Vol-2*, M. Balkanski (ed.) North Holland, Amsterdam, p. 45 (1980).
- [5] T. Thio, J. W. Bennett, D. J. Chadi, R. A. Linke, P. Beela, *J. Cryst. Growth* **159**, 345 (1996).
- [6] J. C. C. Fan, B. J. Palm, *Solar Cells* **12**, 401 (1984).
- [7] T. L. Chu, S. S. Chu, F. Firszt, H. A. Naseem, R. Stawski, B. Xu, 18<sup>th</sup> IEEE Photovoltaic Specialists Conf., New York: IEEE, 1985, p.1643.
- [8] T. M. Rasykov, V. I. Vyalyi, *Appl. Solar Energy* **24**, 1 (1988).
- [9] K. K. Chattopadhyay, A. Sarkar, A. Chaudhuri, A. K. Pal, *Matter. Lett.* **16**, 218 (1993).
- [10] B. Samantha, U. Pal, B. K. Samantaray, S. L. Sharma, A. K. Chaudhuri, *Bull. Mater. Sci.* **18**, 81 (1995).
- [11] J. J. Kennedy, P. M. Amirtharaj, P. R. Boyd, *J. Cryst. Growth* **102**, 266 (1990).
- [12] B. Ragothamachar, H. Chung, M. Dudley, D. J. Larson Jr., *J. Electronic Mater.* **27**(6), 556 (1998).
- [13] T. S. Lee, K. K. Choi, Y. T. Jeoung, H. K. Kim, J. M. Kim, Y. H. Kim, J. M. Chang, W. S. Song, S. U. Kim, M. J. Park, S. D. Lee, *J. Electronic Mater.* **26**(6), 552 (1997).
- [14] T. S. Lee, Y. T. Jyoung, H. K. Kim, J. M. Kim, S. J. Song, S. Y. Ann, J. Y. Lee, Y. H. Kim, S. U. Kim, M. J. Park, S. D. Lee, S. H. Suh, *Proceedings of SPIE* **3436**(1), 67 (1998).
- [15] A. Rohatgi, S. A. Ringel, R. Sudharsanan, P. V. Meyers, C. H. Liu, V. Ramanathan, *Solar Cells* **27**, 219 (1989).
- [16] K. Prasada Rao, O. Md. Hussain, B. Srinivasalu Naidu, P. Jayarama Reddy, *Adv. Matter. for Optics and Electronics* **7**, 109 (1997).
- [17] S. A. Ringel, R. Sudharsanan, A. Rohatgi, M. S. Owens, H. P. Gillis, *J. Vac. Sci. and Technol.* **A8**(3), 2012 (1990).
- [18] B. Samantha, S. L. Sharma, A. K. Chaudhuri, *Vacuum* **46**(1), 739 (1995).
- [19] S. Tolansky, "Multiple-beam Interference Microscopy of Metals", Academic, London, p.55 (1970).
- [20] V. J. Zemski, E. L. Ivshenko, D. N. Mirlin, J. J. Reshina, *Solid State Commun.* **84**, 4448 (1998).
- [21] R. C. Bowman, R. L. Alt, P. M. Adams, J. F. Knudson, D. N. Jamieson, R. G. Downing, *J. Cryst. Growth* **86**, 768 (1998).
- [22] A. M. Ibrahim, *Vacuum* **48**(1), 5 (1998).
- [23] H. S. Soliman, F. M. Allam, A. A. El-Shazly, *J. Mater. Sci. in Electronics* **7**, 233 (1996).
- [24] J. C. Manifacier, J. Gasiot, J. P. Fillard, *J. Phys.* **E9**, 1002 (1976).
- [25] U. Pal, R. Silva-Gonzalez, G. Martinez-Montes, M. Gracia-Jimenez, M. Vidal, S. Torres, *Thin Solid Films* **305**, 345 (1997).
- [26] S. Choudhuri, S. K. Das, A. K. Pal, *Thin Solid Films* **147**, 9 (1987).
- [27] E. Khawaja, S. G. Tomlin, *J. Phys. D: Appl. Phys.* **8**, 581 (1975).
- [28] I. Yu, T. Isobe, M. Senna, *Matter. Res. Bull.* **30**, 975 (1995).
- [29] S. S. Islam, S. Rath, K. P. Jain, S. C. Abbi, *Phys. Rev.* **B46**, 4982 (1992).
- [30] A. S. Pine, G. Dresselhaus, *Phys. Rev.* **B4**, 356 (1971).